Supporting Information for

Multi-Year Global Oscillations in GNSS Deformation and Surface Loading Contributions

Songyun Wang [1,*], Clark R. Wilson [1,2], Jianli Chen [3,4,5], Yuning Fu [6], Weijia Kuang [7], and Ki-Weon Seo [8]

[1]Center for Space Research, University of Texas at Austin, Austin, TX 78759, USA

[2]Department of Earth and Planetary Sciences, Jackson School of Geosciences, University of Texas at Austin, Austin, TX 78712, USA

[3]Department of Land Surveying and Geo-Informatics, The Hong Kong Polytechnic University, Hong Kong, China

[4]Research Institute for Land and Space, The Hong Kong Polytechnic University, Hong Kong, China

[5]The Hong Kong Polytechnic University Shenzhen Research Institute, Shenzhen 518057, China

[6]School of Earth, Environment and Society, Bowling Green State University, Bowling Green, OH 43403, USA

[7]Geodesy and Geophysics Laboratory, NASA Goddard Space Flight Center, Greenbelt, MD 20770, USA

8 Earth Science Education, Seoul National University, Seoul 08826, Republic of Korea

* Correspondence: sywang@csr.utexas.edu

Contents of this file

Table S1
Text S1 and S2
Figures S1 to S12

Introduction

This supporting information contains 1 table, 2 texts and 12 figures, all presented in the order as they are referenced in the main manuscript. Table S1 shows the list of selected 38, 271, and 41 GPS stations. Fig. S1 presents the rapid decrease of loading displacements away from the load. Fig. S2 shows model-predicted loading displacements from different atmospheric models at the 6 example

stations. Texts S1 and S2, accompanied by Figs. S3 to S6, present the results of synthetic experiments with varying stations and harmonic fits, respectively. Fig. S7 is DFT periodogram for [2, 2] GPS series and loading estimates using the 271 stations. Fig. S8 is wavelet spectra of [2, 2] GPS series and loading-corrected estimates using 271 stations. Fig. S9 presents ~6-year sinusoidal fits of [2, 2] vertical displacements at 6 example stations. Figs. S10 and S11 show DFT periodogram of [2, 2] GPS series and loading-corrected series from the four TWS load estimates and two atmospheric models. Fig. S12 shows wavelet spectra of [2, 2] coefficients from GPS daily vertical displacements for comparison with published results.

Table S1. List of selected 38, 271, and 41 GPS stations. The 41 stations are a subset of the 271, indicated in bold font.

38 Stations	271 and 41 Stations							
ALGO	**AGMT**	CDMT	FERN	**KARR**	MSOB	RAMT	TJRN	WWMT
BLYT	**AIRA**	CHMS	FFMJ	KBRC	MTJO	RCA2	TLSE	YAR2
BOR1	**ALBH**	**CHUM**	FGST	**KERG**	NANO	RDMT	TONG	YEBE
BRAN	**ALGO**	**CHUR**	FLIN	**KOKB**	NDAP	RDOM	TONO	**YELL**
BRIB	**ALIC**	CHWK	FMVT	KRAC	NHRG	REDM	TORP	ZIMM
BRMU	**AREQ**	CJMS	FOOT	KTBW	**NKLG**	**REUN**	TOST	
CAS1	**ATW2**	CLGO	FRED	KYVW	NOCO	REYK	**TOW2**	
CMBB	**AUCK**	CMBB	FVPK	**LAMP**	NOPK	RHCL	TRAK	
CRFP	AVRY	CNPP	FZHS	LAPC	NTKA	RIGA	**TRDS**	
DAV1	BALD	COON	GARL	**LAUT**	**NYA1**	RNCH	TRND	
DRAO	BAR1	COPR	**GENO**	LBC1	NYAL	RSTP	TRO1	
FAIR	BARH	CORV	GLSV	LDES	OAES	SAOB	TSKB	
FARB	BBDM	CRBT	GNPS	LEIJ	**OHI2**	SAWC	TWHL	
GODE	BCOV	CRRS	GOBS	LEWI	OPBL	SC02	UCD1	
GRAZ	BEMT	CRU1	GODE	**LHAZ**	OPCP	**SCH2**	UCLU	
JOZE	BEPK	CSCI	GOPE	LINC	ORES	SCIA	USGC	
JPLM	BGIS	CSDH	GOSH	LJRN	ORID	SDHL	USLO	
KERG	BILL	CSST	GRAS	LKCP	ORMT	SEDR	USUD	
KIRU	**BJFS**	CTMS	**HARB**	LL01	ORVB	SELD	VDCY	
KOKB	BKAP	CUHS	HCMN	LMUT	OVLS	SFDM	VIMT	
LAMA	BKMS	CVHS	HERS	LNMT	PALM	SHIN	VNCO	
LBCH	BMHL	DAEJ	HIVI	LORS	PENC	SHOS	VNPS	
LONG	**BOGI**	**DAV1**	HNPS	LROC	PGC5	SLMS	VTIS	
MAC1	BOGO	DDMN	**HOB2**	LVMS	PIE1	SMEL	WATC	
ONSA	BOR1	DHLG	**HOFN**	**MAC1**	PIN1	SOMT	WCHS	

PIN1	BREW	DIAB	HOKI	**MANA**	PIN2	SPMS	WGPP
PIN2	**BRST**	DRAG	HOL3	MAT1	PKDB	**STJO**	WGTN
POTS	**BSHM**	DRAO	HOLB	MAT2	PKRD	SULP	WGTT
QUIN	BSRY	DSSC	HOTK	MATE	PMTN	SUTB	WHYT
STJO	BUCU	DUBO	HUEG	**MAWY**	POL2	SUTH	WIDC
TIBB	BURN	ECFS	HVYS	MEDI	POLV	SUWN	WILL
TMGO	BVPP	ECHO	IMPS	MHMS	PPBF	TABL	WKPK
TRAK	CA99	EDPP	**INVK**	MJPK	PSDM	TAUP	WMAP
TSKB	CABL	EGAN	JOZE	MKEA	PTBB	THCP	WNRA
UCLU	CAGS	ELKO	JPLM	MLFP	PTSG	**THTI**	WOMT
WILL	**CAS1**	EWPP	JRO1	MONP	PVE3	**THU2**	WRHS
YELL	CAST	FAIR	KABR	MPWD	QUIN	TIBB	WTZR
ZIMM	CCCC	FARB	KARA	MQZG	RAMO	TILC	WTZZ

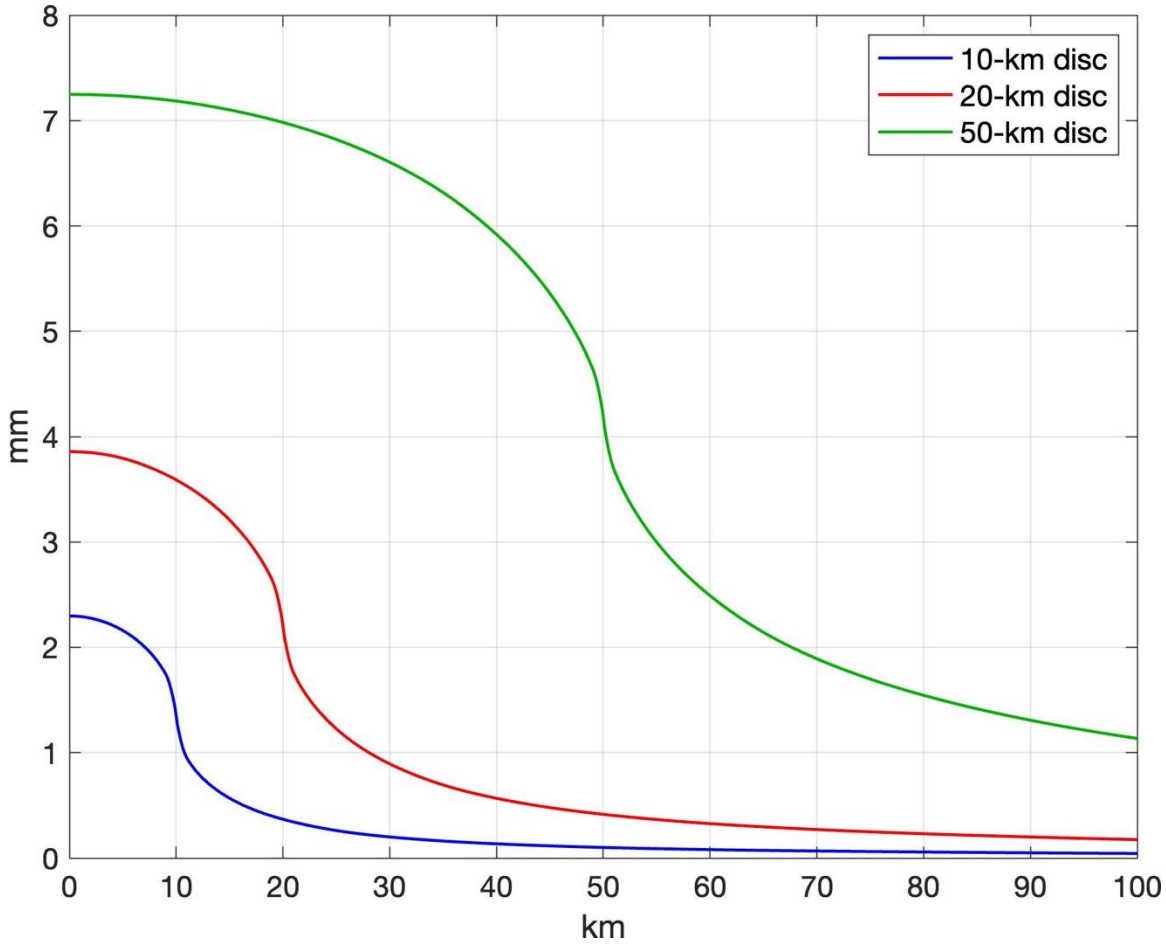


Figure S1. Vertical displacements caused by the removal of a uniform disc load of 1 m equivalent water thickness, with disc radii of 10 km (blue curve), 20 km (red curve), and 50 km (green curve), plotted as a function of the distance from the disc center.

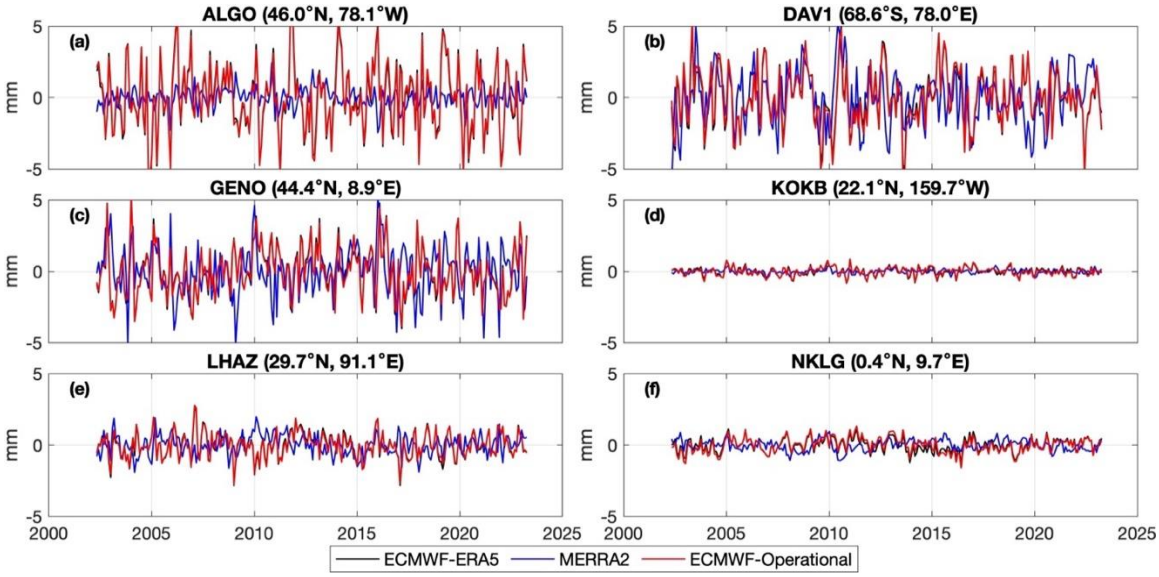


Figure S2. Atmospheric load time series over the continents from ECMWF-ERA5, MERRA-2, and ECMWF-Operational at stations (a) ALGO, (b) DAV1, (c) GENO, (d) KOKB, (e) LHAZ, and (f) NKLG. Annual and semi-annual terms, and linear trends have been removed.

Text S1

Figs. S3a to S3c show DFT periodogram spectra of $C_{22} + iS_{22}$ for the true (red curves) and ensemble means of estimates (black curves) using 38, 271, and 41 stations. In Fig. S3 all coefficients from degrees 0 to 2 are fit. The LSQ annual, semi-annual components and linear trends have been removed, and a 2 to 8-year zero phase band-pass Butterworth filter has been applied prior to spectral analysis. The gray area contains the 3σ confidence region of the ensemble of 100. These results show that using 271 stations has an advantage in suppressing random observation noise, thus reducing areas of the 3σ confidence regions. The discrepancy between black and red curves in Fig. S3a indicates that with only 38 stations there is an overestimation of power by 10 to 20 dB. Overestimation is reduced using both 271 and 41 stations, suggesting the effect may be related to uneven geographical distribution of the 38 stations.

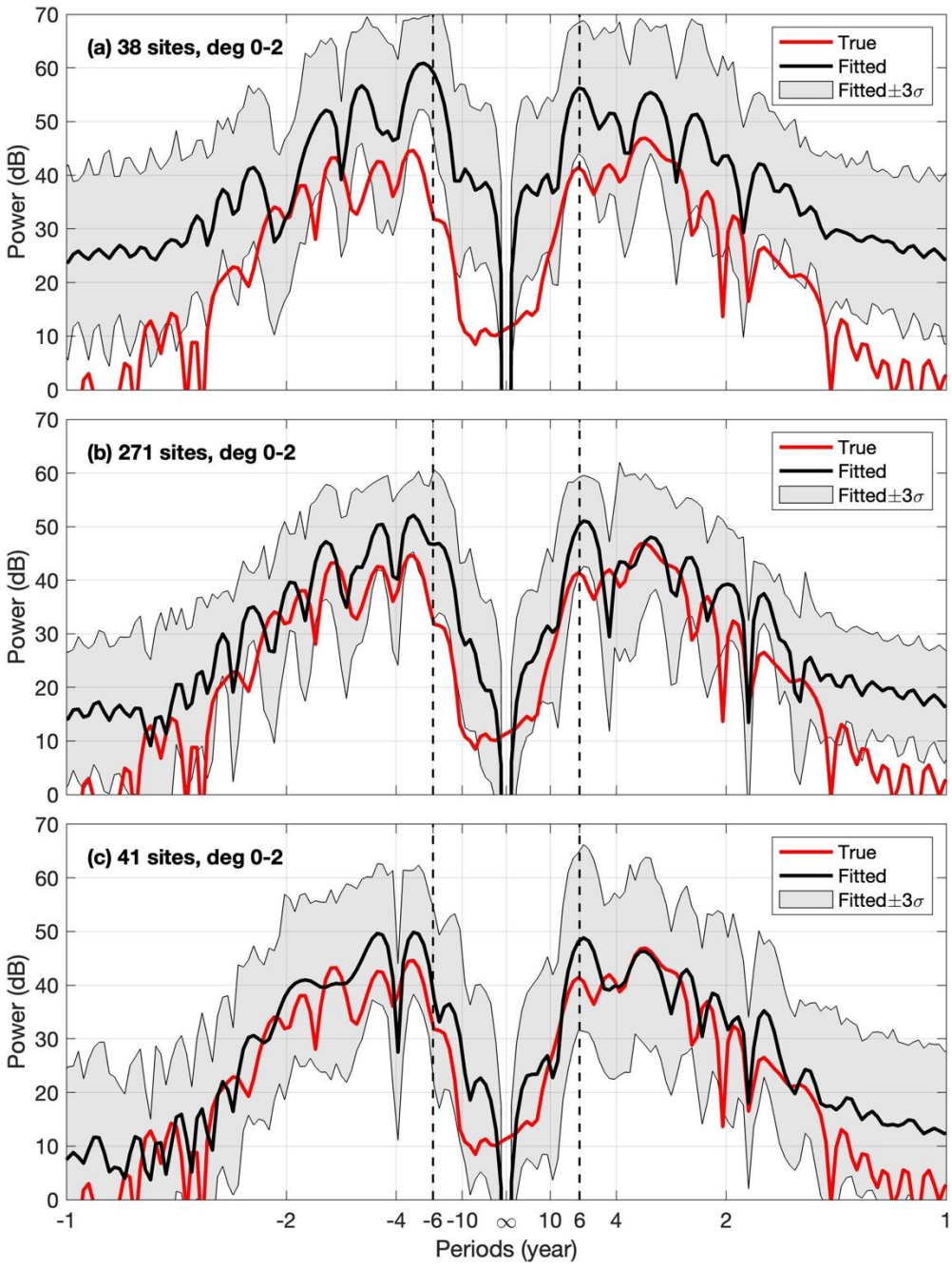


Figure S3. DFT periodograms of $C_{22} + iS_{22}$: true (red) and ensemble means of LSQ estimates (black) with randomly generated flicker noise at (a) 38 sites, (b) 271 sites, and (c) 41 sites. The gray area contains the 3σ confidence region. Station data are latitude weighted as described in the text, and all coefficients from degrees 0 to 2 are estimated simultaneously. A 2 to 8-year band-pass filter has been applied prior to spectral analysis.

The real-valued Morlet wavelet spectra of [2, 2] coefficients which reveal the same dominant signals as in DFT periodogram (i.e., near ±3- and ±6-year periods) are shown in Fig. S4. The two

panels in the first row correspond to the true signals (red curves in Fig. S3), while panels from the second to fourth rows are estimates (black curves in Fig. S3) from 38, 271, and 41 stations, respectively with retrograde (left column) and prograde (right column). The dominant signals near ±3- and ±6-year periods are evident in each case. Overestimation of power occurs in all three cases but using more evenly distributed stations mitigates this issue to some extent. Differences in times and magnitudes of amplitude are observed in Fig. S4 in all three cases. These differences may be related to regional signals associated with particular GPS stations, and are investigated using real GPS data in main text Section 3.2.

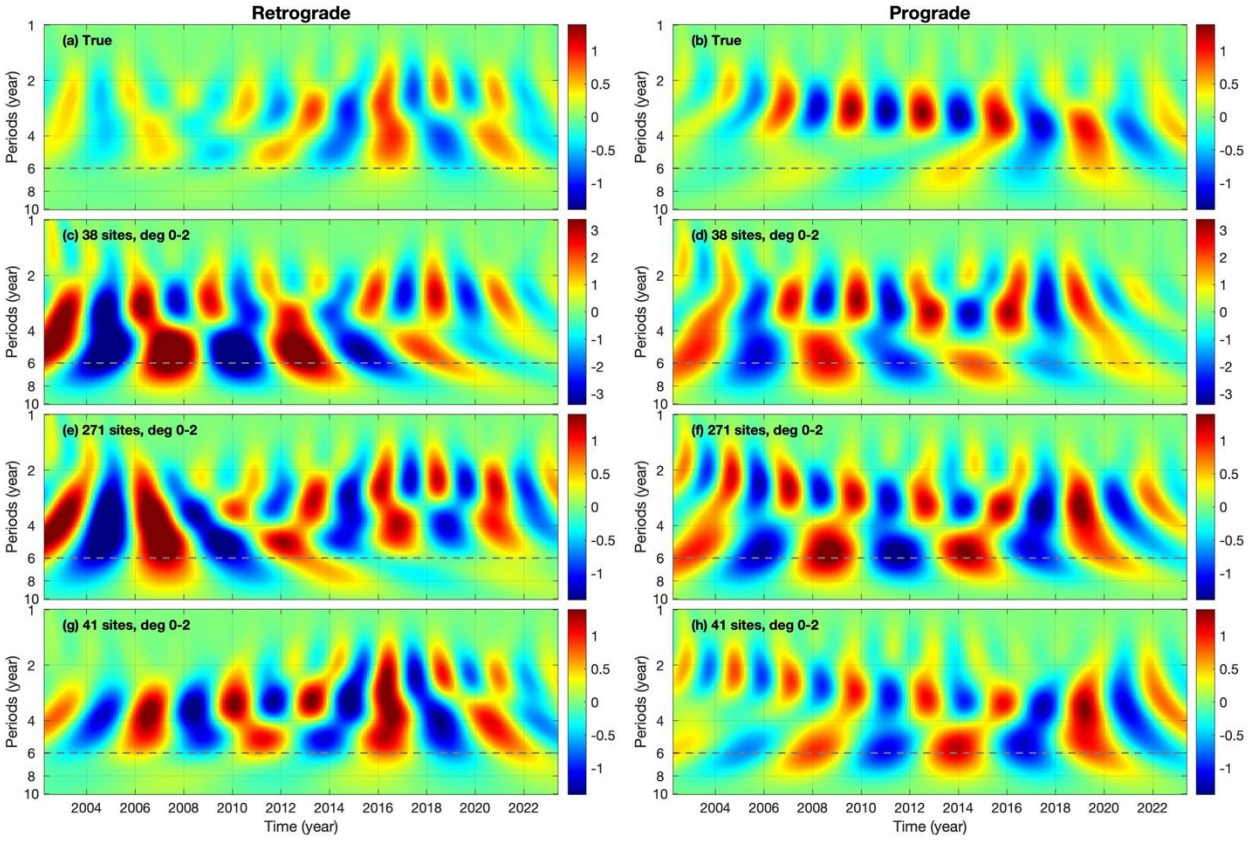


Figure S4. Wavelet spectra of band-pass filtered $C_{22} + iS_{22}$ LSQ fit to vertical displacements in synthetic data experiments using various sets of station locations. Retrograde signal spectra are in the left column (a, c, e, g) and prograde in the right column (b, d, f, h). (a) and (b) are Morlet spectra for the true coefficients; (c) and (d) are results estimated from 38 station; (e) and (f) are from 271 stations; and (g) and (h) are from 41 stations. All coefficients from degrees 0 to 2 are estimated simultaneously. Spectral magnitudes have been scaled by 1×10^{11}. Note that color scales in (c) and (d) are wider than in other panels.

Text S2

Fig. S5 shows DFT periodogram spectra of $C_{22} + iS_{22}$ for the true (red curve) and ensemble means of the estimates (black curves) using 271 stations. Figs. S5a to S5c illustrate the results when all coefficients are fit to degree 2 only, degrees 0 through 2, and degrees 0 through 3. A 2- to 8-year zero-phase band-pass Butterworth filter has been applied prior to spectral analysis. The gray area contains the 3σ confidence region of the ensemble of 100. These results show that fitting coefficients from degrees 0 through 3 results is less effective in suppressing random noise, as evidenced by the larger 3σ confidence regions.

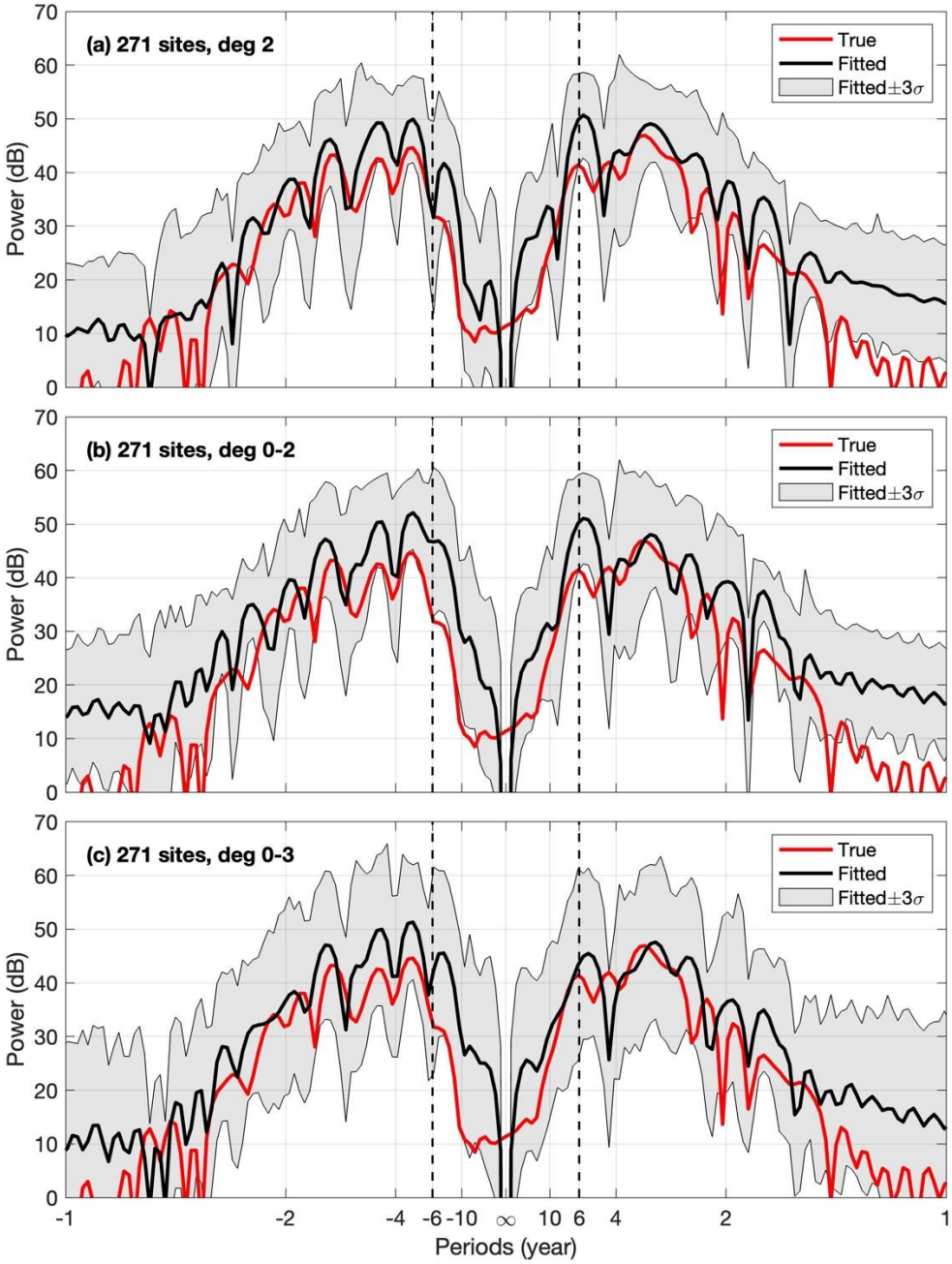


Figure S5. DFT periodograms of $C_{22} + iS_{22}$: true (red) and ensemble means of LSQ estimates (black) with randomly generated flicker noise at 271 sites. All coefficients from (a) degree 2 only, (b) degree 0 through 2, and (c) degree 0 through 3 are estimated simultaneously. The gray area contains the 3σ confidence region. Station data are latitude weighted as described in the text. A 2- to 8-year band-pass filter has been applied prior to spectral analysis.

Fig. S6 shows real-valued Morlet wavelet spectra of [2, 2] coefficients. The two panels in the first row correspond to the true signals (red curve in Fig. S5), while panels from the second to

fourth rows are for estimates (black curves in Fig. S5) when fitting degree 2 only, degrees 0 through 2, and degrees 0 through 3, for retrograde (left column) and prograde (right). Overestimation of power occurs in all three cases. The wavelet spectra for the first two cases (degree 2 only and degrees 0 through 2) are quite similar, showing similar strong variations near ±3- and ±6-year periods. Fitting degrees 0 through 3, causes other variations near –8 years to appear.

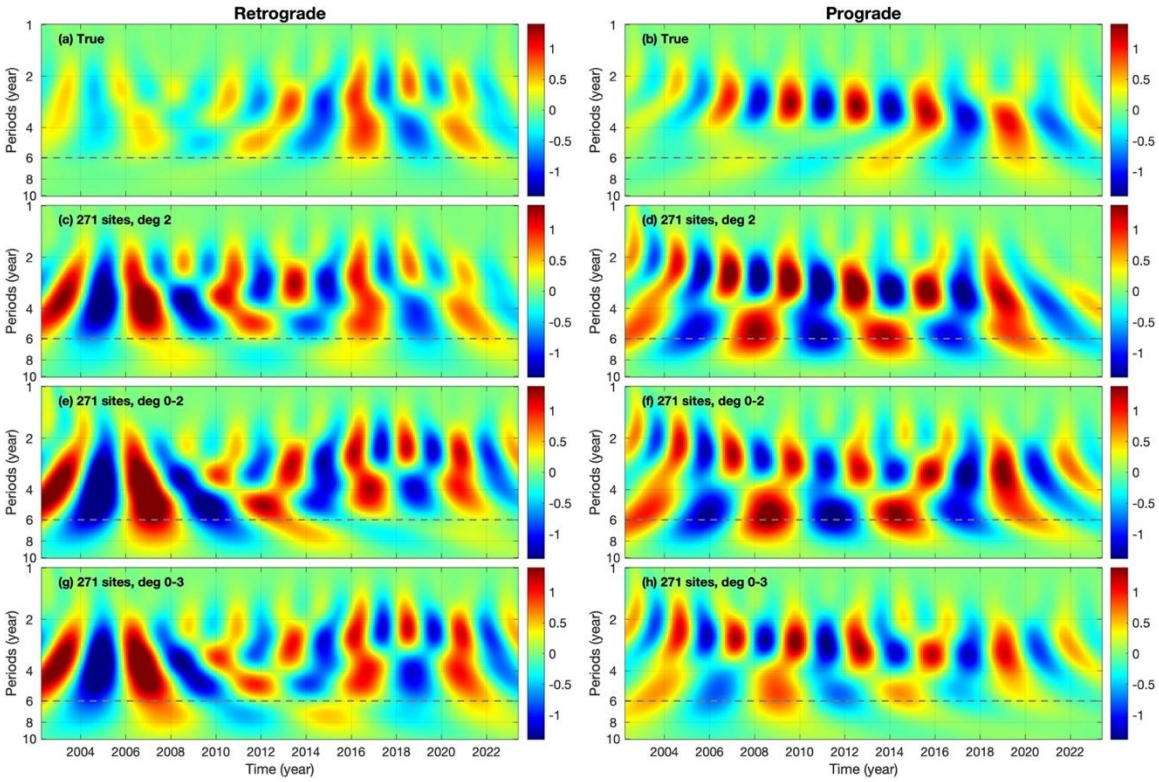


Figure S6. Wavelet spectra of band-pass filtered $C_{22} + iS_{22}$ estimated from 271 GPS station vertical displacements using various sets of fitting coefficients. Retrograde signal spectra are in the left column (a, c, e, g) and prograde in the right column (b, d, f, h). (a) and (b) are Morlet spectra for the true coefficients; (c) and (d) estimate all coefficients of degree 2 only; (e) and (f) estimate all coefficients from degree 0 to 2; and (g) and (h) estimate all coefficients from degree 0 to 3. Spectral magnitudes have been scaled by 1×10^{11}.

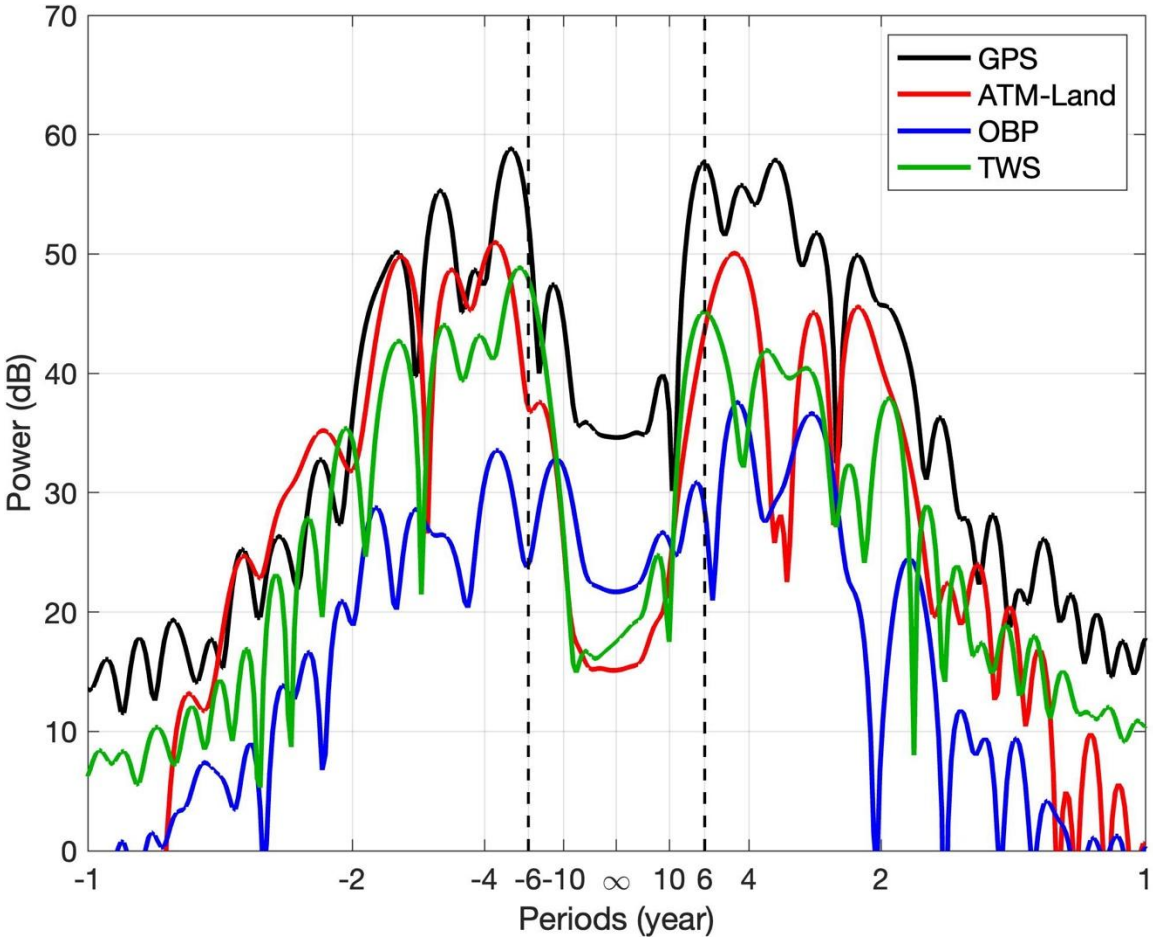


Figure S7. DFT periodograms of $C_{22} + iS_{22}$ estimated from 271 GPS station vertical displacements (black curve) and individual vertical loading displacements from different sources (colored curves).

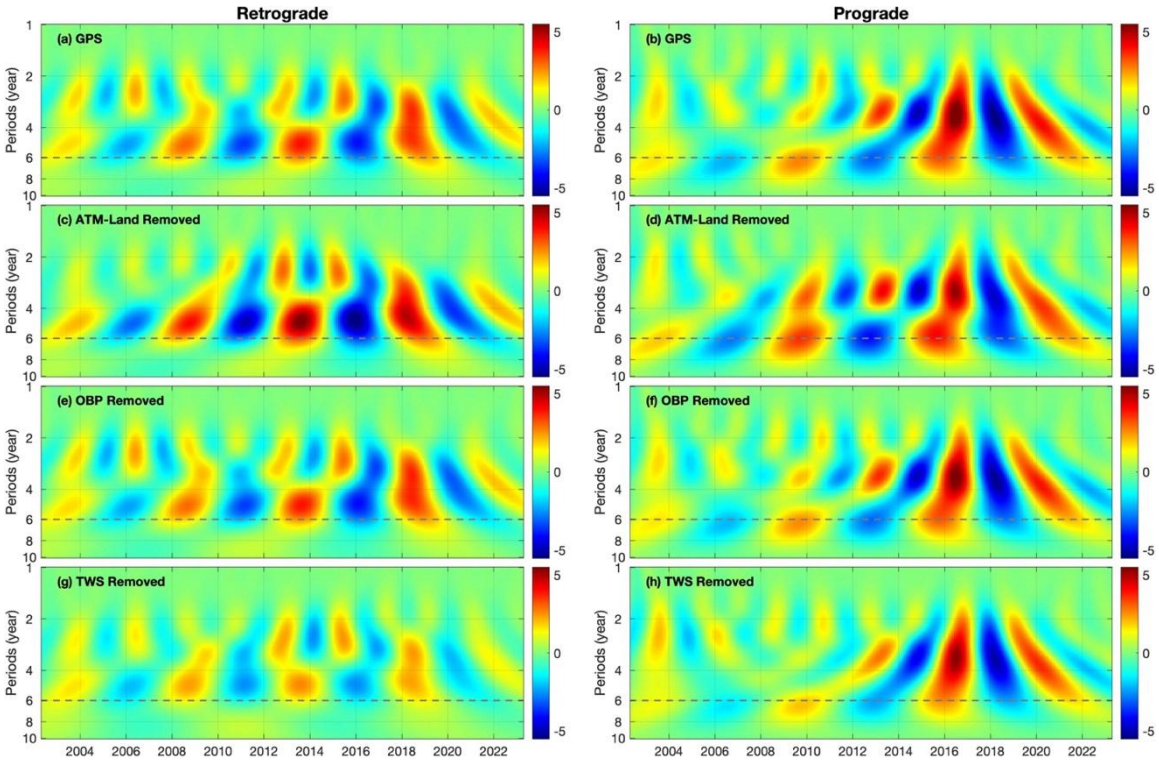


Figure S8. Wavelet spectra of band-pass filtered $C_{22} + iS_{22}$ estimated from 271 GPS station vertical displacements with loading removed. Retrograde and prograde signals are shown in the left and right columns, respectively. (a) and (b) derive from GPS vertical displacements; (c) and (d) from GPS minus atmospheric loading over the continents; (e) and (f) from GPS minus OBP loading; (g) and (h) from GPS minus TWS loading. Spectral magnitudes have been scaled by 1×10^{11}.

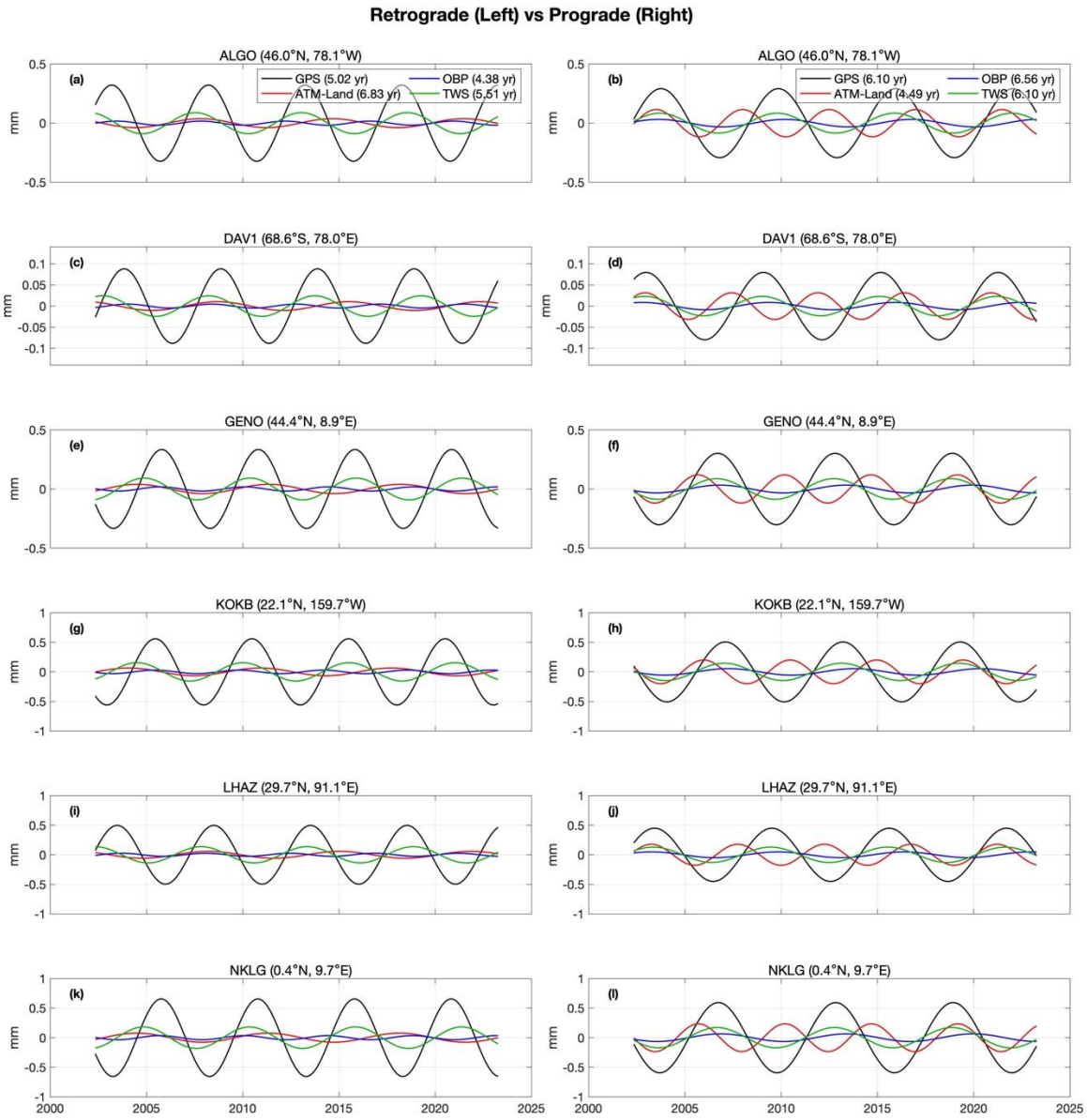


Figure S9. LSQ fit sinusoids for retrograde (left) and prograde (right) SYO in [2, 2] vertical displacements from 271 GPS station vertical displacements (black curves), atmospheric loading over the continents (red curves), OBP loading (blue curves), and TWS loading (green curves) at (a) and (b) ALGO, (c) and (d) DAV1, (e) and (f) GENO, (g) and (h) KOKB, (i) and (j) LHAZ, and (k) and (l) NKLG. Sinusoidal periods closest to ±6-years are identified from the respective DFT periodogram in Fig. S7.

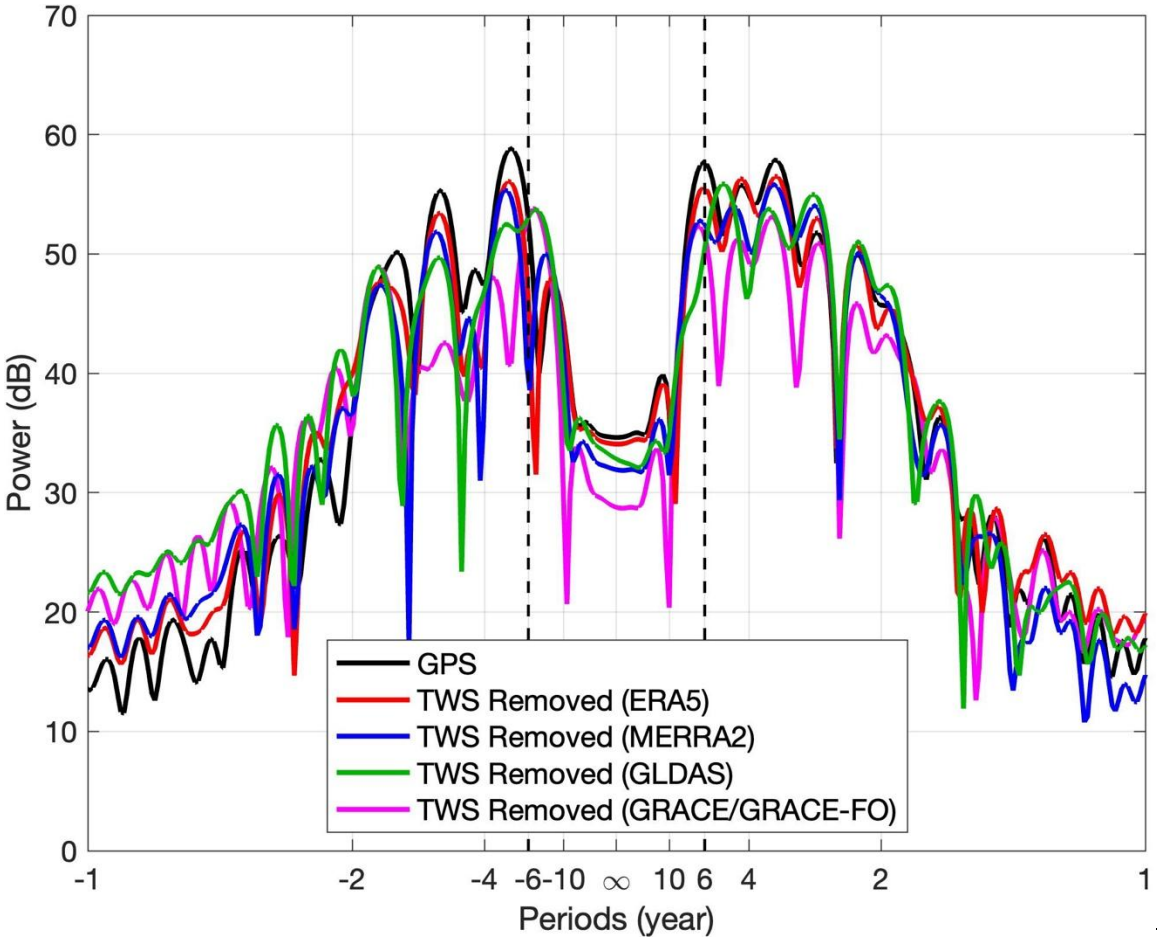


Figure S10. DFT periodogram of $C_{22} + iS_{22}$ estimated from 271 GPS station heights (black curve) and GPS minus TWS loading using ERA5 (red curve), MERRA2 (blue curve), GLDAS (green curve), and GRACE/GRACE-FO (magenta curve) models/observations.

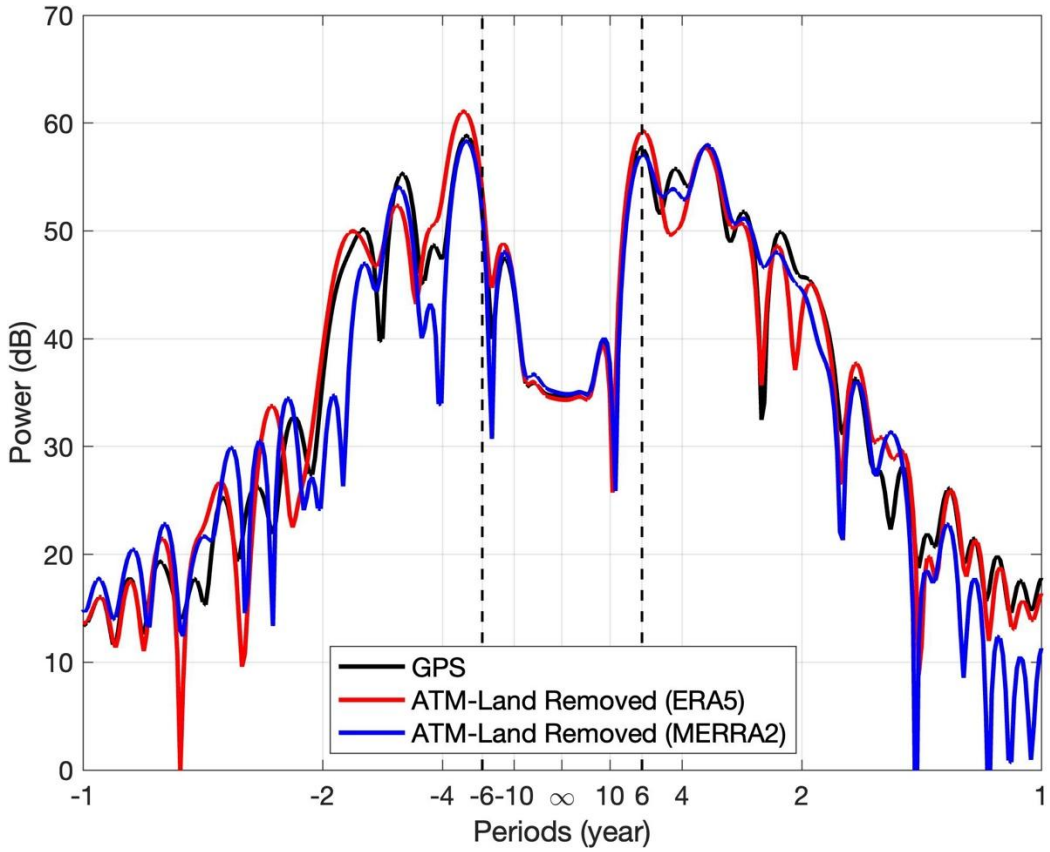


Figure S11. DFT periodogram of $C_{22} + iS_{22}$ estimated from 271 GPS station heights (black curve) and GPS minus atmospheric loading over the continent using ERA5 (red curve) and MERRA2 (blue curve) models.

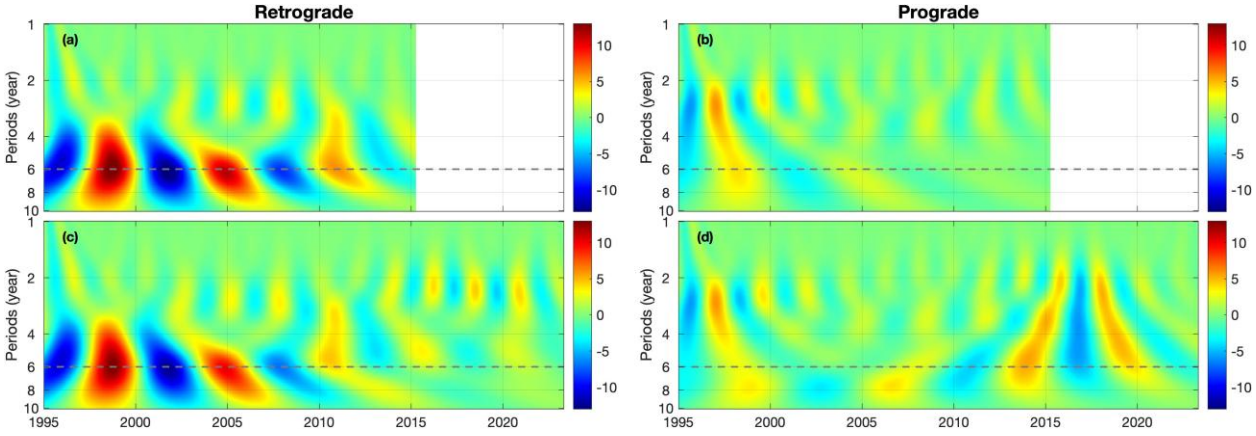


Figure S12. Wavelet spectra of band-pass filtered $C_{22} + iS_{22}$ estimated from 35 GPS station daily vertical displacements. A reversed sign of GPS vertical displacement is applied (for consistency with Ding & Chao (2018)). Retrograde and prograde signals are shown in the left and right columns, respectively. (a) and (b) are from Jan. 1995 to Apr. 2015; (c) and (d) are from Jan. 1995 to Apr.

2023. Spectral magnitudes have been scaled by 1×10^{11}. Fig. S12a bears a strong resemblance to Fig. 3b in Ding & Chao (2018).